

Article

Crystal Engineering for Mechanical Strength at Nano-Scale Dimensions

Ronald W. Armstrong 

Department of Mechanical Engineering, University of Maryland, College Park, MD 20742, USA; rona@umd.edu; Tel.: +1-410-723-4616

Academic Editor: Shujun Zhang

Received: 22 September 2017; Accepted: 15 October 2017; Published: 18 October 2017

Abstract: The mechanical strengths of nano-scale individual crystal or nanopolycrystalline metals, and other dimensionally-related materials are increased by an order of magnitude or more as compared to those values measured at conventional crystal or polycrystal grain dimensions. An explanation for the result is attributed to the constraint provided at the surface of the crystals or, more importantly, at interfacial boundaries within or between crystals. The effect is most often described in terms either of two size dependencies: an inverse dependence on crystal size because of single dislocation behavior or, within a polycrystalline material, in terms of a reciprocal square root of grain size dependence, designated as a Hall-Petch relationship for the researchers first pointing to the effect for steel and who provided an enduring dislocation pile-up interpretation for the relationship. The current report provides an updated description of such strength properties for iron and steel materials, and describes applications of the relationship to a wider range of materials, including non-ferrous metals, nano-twinned, polyphase, and composite materials. At limiting small nm grain sizes, there is a generally minor strength reversal that is accompanied by an additional order-of-magnitude elevation of an increased strength dependence on deformation rate, thus giving an important emphasis to the strain rate sensitivity property of materials at nano-scale dimensions.

Keywords: crystal (grain) size; nanomaterials; mechanical strength; Hall-Petch relation; dislocation pile-ups; patented steel wire; non-ferrous materials; nano-twinned material; superalloys; composites; strain rate sensitivity

1. Introduction

The strong increase in the mechanical strength of materials at nano-scale dimensions is an important research activity involving tests on both individual crystals and polycrystalline samples. Such strength levels, that are achieved for individual nanoparticles, or as thin films, micropillars, or other polyhedral-shape crystals, also frequently involve the employment of nano-testing systems, such as electron microscopic ‘in situ’ observations or nanoindentation hardness testing, and, perhaps most often, involves determining the strength properties of bulk materials composed of nano-scale crystal constituents. No less important is the current research effort applied to understanding the reason(s) for the superior strength levels. The present report contributes to the effort by providing a dislocation-mechanics-based analysis of such crystal strength properties, either when seemingly un-constrained, but especially, when internally constricted within a larger polycrystalline microstructure. Current measurements are provided on body-centered cubic (bcc) iron and steel materials, then leading to consideration of face-centered cubic (fcc) and hexagonal close-packed (HCP) metals and polyphase superalloys and composite example materials.

2. Nanocrystal/Nanopolycrystal Strengths of Iron and Steel

As mentioned, the testing of individual nanocrystals often requires comparable-sized engineering test systems and special force and displacement measuring capabilities, as compared to conventional test systems being suitable for bulk materials containing nano-scaled constituents.

2.1. Un-Constrained Nanocrystals

A strength of ~10.7 GPa has been reported for ambient temperature compression tests made on “free-standing” spherical iron nanoparticles with diameters in the range from several tens to over 200 nm and exhibiting a Young’s modulus, E , of 221 GPa [1]. The particles were reported to have a thin (γ -Fe₂O₃) oxidation layer of 4 nm proposed to hinder surface nucleation of dislocations. Force-displacement curves arising from nanoindentation measurements exhibited essentially elastic loading until the sudden plastic collapse. Copious defects, as well as deformation-twinning-like structures, were observed in the catastrophically yielded particles. The measurements were compared to a tensile strength of 13.4 GPa reported for an iron “whisker”. The method of testing relates to measurements reported for silicon nanospheres of comparable dimensions, also oxide film encased, and interpreted using a Hertzian nanoindentation basis [2]. Very importantly, an inverse dependence of strength on crystal size was found. In general, such inverse size effect is attributed to the stress for nucleation or growth of a dislocation loop of diameter, ℓ , taken equal to the crystal diameter. The tensile or compressive strength, σ_ℓ , dependence on ℓ , to be further employed in the present report for pile-up of circular dislocation loops [3], is given as

$$\sigma_\ell = m_T[\tau_0 + (3Gb/4\pi\ell)\{(5/6)(\ln[4\ell/b] - 1) - [1/16]\}] \quad (1)$$

In Equation (1), m_T is a Taylor orientation factor to connect with operation of a relevant shear stress, τ_0 is a ‘friction shear stress’ required for dislocation movement, G is shear modulus, and b is dislocation (displacement) vector. In a follow-up report to the spherical silicon nanoparticle measurements, a report was made on the compression of silicon nanocubes in which internal dislocation pile-ups were hypothesized [4]. Important evidence for their presence came from the recovered backward flow on unloading of the piled-up dislocations, seen to occur in slip band structures traversing between the top and bottom constraints of the compression test platens. Credit was given to the pioneering analysis of Eshelby, Frank, and Nabarro (EFN) for the description of pile-up parameters employed in the assessment of the measurements [5]. The EFN description had led Hall and Petch to a pioneering derivation of a reciprocal square root of ℓ dependence for the lower yield and cleavage fracture strengths of low carbon steel materials in the H-P relationship [6,7]:

$$\sigma = \sigma_{0i} + k_i\ell^{-1/2} \quad (2)$$

In Equation (2), the experimental constants, σ_{0i} and k_i with subscript index “i” are $\sigma_{0l.y.p.}$ and $k_{l.y.p.}$ for the lower yield point and are σ_{0C} and k_C for cleavage.

2.2. Constrained Polycrystalline Plasticity

In line with Equation (2), Figure 1 provides a comparative graph of measurements made on various iron and steel materials. The figure is a latest extension of an earlier version in which the labeled Armstrong et al. results were described and the top, delineated, theoretical strength was taken as $E/30$ [8]. The current measurements cover on a log/log basis the size dependence of strength based on the following effective length scales: the average grain diameter for conventional 0.15 wt % carbon mild steel and other decarburized [9], IF (interstitial-free) iron [10], and ball-milled iron [11] materials; the lamellar spacing for eutectoid (pearlitic) iron-Fe₃C (iron carbide) wire [12,13]; and, the subgrain boundary spacing for the topmost hypereutectoid wire material measurement [14], which strength level falls coincidentally at the previously estimated value of $E/30$. One might also note that the solid

and dashed curves beginning from largest length scale follow a $(1/\ell)^{1/2}$ dependence beginning from different levels of the σ_0 value specified in Equation (2). At its smallest size, the solid inverted-triangle and open-circle points at smallest size give indication of transition from a $(1/\ell)^{1/2}$ dependence for Equation (2) to a $(1/\ell)$ dependence for Equation (1); see the drawn-in top-right-triangle of unit slope based on the length scale.

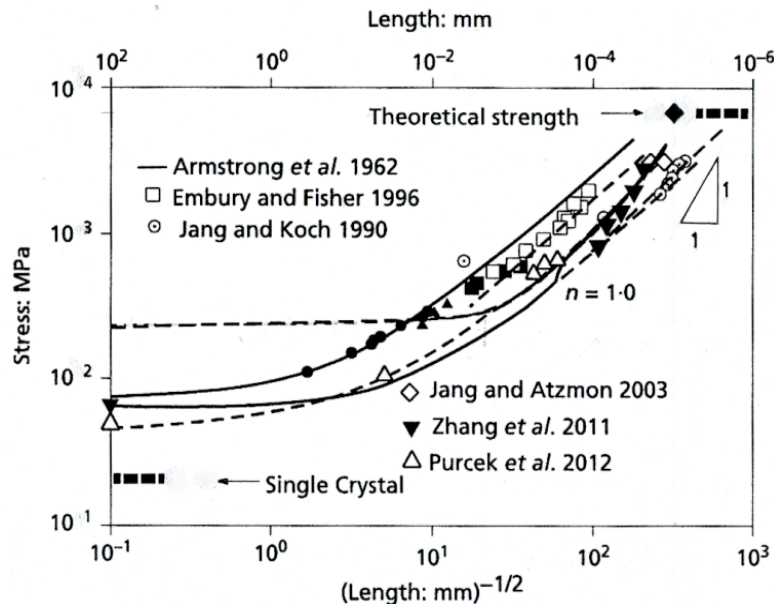


Figure 1. The strength dependence on crystal (grain) size for a number of iron and steel materials: mild steel; decarburized (Swedish) iron; pearlitic steel; ball-milled iron; interstitial-free (IF) iron; and, (patented) eutectoid and hypereutectoid steel wire.

Table 1 provides a list of relevant σ_0 and k values for all of the data [15] in Figure 1 except for the newly-added closed-diamond point at a highest strength level of ~ 7 GPa and at a measured smallest (subgrain) spacing of ~ 9 nm that was reported to determine the strength level [14]. In Table 1, the flow stress at true strain, $\epsilon = 0.1$, gives indication of raising, $\sigma_{0\epsilon}$, and reducing k_ϵ after the lower yield point (Lueders) extension. The smaller k values for the decarburized iron, ball milled iron, and IF iron measurements, as compared to the mild steel value, illustrate the lesser constraining effect produced at grain boundaries by reduction in the carbon content. A recent report has been made on different aspects of carbon segregation at individual dislocations and relating to pile-ups at grain boundaries [16]. Such segregation applies also for high manganese (fcc) austenitic steels [17]. Fitzgerald and Dudarev have given dislocation pile-up calculations for fcc gamma-iron based on the EFN model and including an important influence of elastic anisotropy [18].

Table 1. Hall-Petch parameters for iron and steel materials.

Material/Method	σ_0 (MPa)	k (Mpa.mm ^{1/2})	τ_c (MPa)
Mild steel, l.y.p.	71	23.4	771
$\epsilon = 0.1$ flow stress	294	12.4	
Decarburized iron	36.3	6.5	
Pearlitic steel	~ 30	~ 19.7	
Ball milled iron	40	7.2	
IF iron	43	11	
$\epsilon = 0.002$ wire	60–1210	6.9–12.7	63–214

Original work from the author.

The local shear stress at a pile-up tip is included in the H-P model description as [19]

$$k_{\epsilon} = m_{\Gamma}(\pi m_{\text{S}} G b \tau_{\text{C}\epsilon} / 2\alpha)^{1/2} \quad (3)$$

In Equation (3), m_{S} is a Sachs orientation factor, $\tau_{\text{C}\epsilon}$ is the local shear stress at the pile-up tip, and $\alpha \approx 0.84$ is for an average dislocation character. Several estimates of $\tau_{\text{C}\epsilon}$ are given on the top and bottom lines of Table 1. In comparison with the top value, a $\tau_{\text{C}\epsilon} = 0.83$ GPa had been estimated for conventional grain size measurements [19]. The lower $\tau_{\text{C}\epsilon}$ values given in Table 1 relate to the predicted transition to a $(1/\ell)$ dependence for the reported steel wire measurements, and here, the range in $\tau_{\text{C}\epsilon}$ values relates to several ways described in [13] of accounting for the strength properties in terms of different $\sigma_{0\epsilon}$ and k_{ϵ} values.

The natural limit for reduction in pile-up size is given by one dislocation loop expanding against the grain boundary resistance. Such estimation corresponds to the EFN condition for number of dislocation loops in a circular pile-up, $n = 1.0 \approx (2\alpha k_{\epsilon} \ell^{1/2} / \pi m_{\Gamma} G b)$. The single loop pile-up condition is obtained by modifying Equation (1) to include the addition of $m_{\Gamma} \tau_{\text{C}\epsilon}$ to overcome the grain boundary resistance as

$$\sigma = \sigma_{\ell} + m_{\Gamma} \tau_{\text{C}\epsilon} \quad (4)$$

In Equation (4), the value of $\tau_{\text{C}\epsilon}$ is obtained from Equation (3) by employing the known value of k_{ϵ} . The $n = 1.0$ condition is shown in Figure 1 to occur just below the observed turn-up in strength observed for the Zhang et al. [13] (filled-inverted-triangle) measurements. Interestingly, the indicated trend of the $(1/\ell)$ dependence in Figure 1 points to the plotted position of highest strength level reported for the filled-diamond measurement. Notably, the transition at $n = 1.0$ depends on k_{ϵ} in Equation (3), and thus, is moved to smaller ℓ as k_{ϵ} is larger. Thus, for example, the mild steel and open-square pearlitic steel wire results with larger k_{ϵ} values are unaffected. Previous indication had been given by Langford for a possible $(1/\ell)$ dependence for other pearlitic wire results [20]. Admittedly, however, the highest strength result obtained in [14] was obtained in a relatively more complicated situation and the subgrain spacing was taken in that report as the effective grain size to fit a raised H-P dependence in Equation (2). Under the condition of such severe drawing, the Fe_3C carbide phase, that anyway is thermodynamically unstable, was found to dissolve in a carbon-supersaturated ferrite phase that then evolved into a final stabilized columnar, nano-scale, subgrain boundary structure with segregated carbon, thus producing the present suggested changeover to a $(1/\ell)$ dependence of the resultant strength.

2.3. Severe Plastic Deformation (SPD)

The role of severe plastic deformation in achieving exceptional grain size refinement with consequent high strength levels at nano-scale dimensions, as exhibited, for example, by the severely drawn wire materials, is an important engineering accomplishment. Muñoz, Higuera, and Cabrera have reported values of $\sigma_{\text{oy}} = 122$ MPa and $k_{\text{y}} = 11.4$ MPa·mm^{1/2} for ARMCO iron processed by equal channel angular pressing (ECAP) and leading to a highest value of $\sigma_{\text{y}} \approx 0.9$ GPa at $\ell \approx 300$ nm [21]. Pioneering work has been done by Valiev and colleagues on ECAP and other processing methods of severe plastic deformation (SPD), dedicated to the production of bulk steel and other metal and alloy materials [22]. These researchers have given a comprehensive description on the obtainment of nanograins, nanoclusters, and nanotwins, and especially on the obtainment of high dislocation densities from forced extrusion conditions involving ϵ values of ~ 4 – 6 [23]. The high dislocation densities contribute to raising both $\sigma_{0\epsilon}$ and the strain hardening property generally measured by $(d\sigma_{0\epsilon}/d\epsilon)$ and, hence, also contribute to increasing the material ductility. An enhanced fatigue endurance and the occurrence of superplasticity was described in [22,23] for a variety of nano-size grain and grain boundary structures.

As indicated, emphasis had been given in [14] to the ultrahigh strength produced by SPD being associated with a high density of dislocations that transformed to a final columnar subgrain

structure that, in turn, was stabilized by the high carbon content of the hypereutectoid steel containing 0.98 wt % carbon. A similar report has been made for achievement of a tensile strength of 2.5 GPa for a medium carbon steel of 0.45 wt % carbon first quenched to body-centered tetragonal martensite and then processed by SPD via high-pressure torsion [24]; thus, adding deformation-induced phase transformation into the engineering tools available to some materials for improving strength properties. In this case, the strength was attributed largely to two sources: stronger grains via solid solution strengthening and an increased dislocation density, both strengthening terms being in σ_0 in Equation (2); and, because of grain boundary strengthening, in the $k\ell^{-1/2}$ term. Such complication is added-to also by the employment of alloying elements, such as manganese, to produce SPD-induced transformation to martensite then to be subjected to appropriate annealing or tempering treatment [25,26]. In [26], emphasis was given to the resultant structure being achieved by deformation via transformation-induced plasticity associated with structural partitioning, thus also allowing the achievement of an increased ductility for the material.

3. Nanopolycrystal FCC Metals

Simulated partial dislocation nucleation at the surface vertices of polygonal, defect-free, fcc metal nanoparticles has been reported [27]. A modified 0.66 power-exponent for the inverse size dependence was obtained. Otherwise, an order-of-magnitude increase in strength level occurs also for nanopolycrystal fcc metals, as well, as demonstrated in the log/log plot of Figure 2 that has been compiled from reported measurements made on aluminum, nickel and copper materials [28–33].

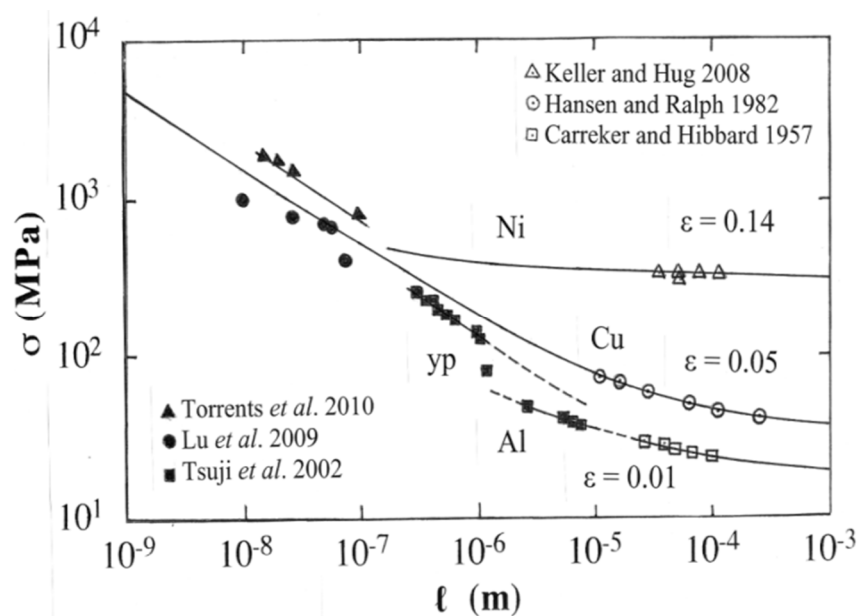


Figure 2. Comparison at conventional and ultrafine grain sizes of H-P measurements for aluminum, copper and nickel.

3.1. Nanograin and Nanotwin Strengthening

In Figure 2, the several H-P-described conventional grain size results are extended to join with counterpart ultrafine grain size measurements. For the aluminum measurements, a transition is shown from a conventional grain size determination of $k_{0.002} = \sim 2.3 \text{ MPa}\cdot\text{mm}^{1/2}$ to a higher $k_{\epsilon} = \sim 4.8 \text{ MPa}\cdot\text{mm}^{1/2}$ value associated with yield point behavior, in the analogous manner already mentioned for the iron and steel materials listed in Table 1, rising to a highest value of $k_{1.y.p.} = 23.4 \text{ MPa}\cdot\text{mm}^{1/2}$. The nickel measurements at conventional grain size gave an initial proof stress $k_{0.002} = \sim 5.2 \text{ MPa}\cdot\text{mm}^{1/2}$ as compared to the hardness-determined $k_{0.075} = \sim 6.2 \text{ MPa}\cdot\text{mm}^{1/2}$

applicable for the ultrafine grain size measurements. In this case for conventional grain size nickel measurements, a relatively rare reduction in k_ϵ to $2.15 \text{ MPa}\cdot\text{mm}^{1/2}$ was obtained at $\epsilon = 0.14$. The indicated H-P dependence at nano-scale grain sizes for copper was reported for compiled measurements [33] and, as will be shown, these data were (to be) matched with nanotwin measurements, in which the nanotwin spacing was taken to produce a same type H-P dependence until reaching a smallest spacing of $\sim 20 \text{ nm}$ and thereafter showing grain size weakening at smaller twin spacings, not untypical of other nano-scale grain size measurements.

The different values of k_ϵ for the fcc metals have been explained on the basis that cross-slip is required for the transmission of plastic flow at the crystal grain boundaries [34]. Connection was made in Equation (3), with single crystal shear stress measurements for cross-slip, that is, with the value of $\tau_{C\epsilon} = \tau_{III}$, the single crystal shear stress for cross-slip. Thus, aluminum, demonstrably exhibiting easy cross-slip, has a lowest $k_\epsilon \geq 1.2 \text{ MPa}\cdot\text{mm}^{1/2}$ value, whereas an approximately same value of k_ϵ for nickel and copper is obtained because the lower τ_{III} for nickel, as compared to copper, compensates in Equation (3) for the lower copper value of G .

Much of the current research on the H-P relationship, and on the dislocation pile-ups that provide the basis for it, is being done at the micro- or nano-scale level. An important illustration was provided by Kapp, Kirchlechner, Pippan, and Dehm [35] in bend tests of bicrystalline copper microcantilevers deformed in-situ under observation with a scanning electron microscope. Slip bands, observed as terminating surface ledges, were observed to be blocked as they approached a bicrystal grain boundary running along the length of the beam. As previously noted for the silicon nano-cube strain recovery observations [4], Kapp et al. associated the obtainment of very significant (Bauschinger-type) strain recovery measurements in their experiments to occur by (backward) relaxation of dislocation pile-ups. In another case, the depth dependence of nanoindentation hardness impressions placed adjacent to an Fe-2.2 wt % Si bicrystal boundary was employed to monitor the transmission of slip through the boundary [36]. In the report, H-P dependence was obtained in accordance with the EFN description for an estimated pile-up length of 200 nm and effective shear stress of 1.5 GPa . The important experiment and analysis were followed-up more recently by another research group [37] presenting a theoretical model description involving the boundary impeding the pile-up of geometrically necessary dislocations produced by the nanoindentations. Similar measurements had been reported for a copper bicrystal grain boundary, including an important consideration of the indentation rate dependence [38]. A discrete dislocation dynamics model description relating the H-P dependence to grain boundary penetrability has been reported [39].

Figure 3 shows relation of copper nanotwin measurements of Lu et al. [33] fitting extrapolation of the conventional grain size measurements reported by Hansen and Ralph [32], whose measurements were also shown in Figure 2. The predicted H-P transition to single loop behavior in this case at $\ell = \sim 100 \text{ nm}$, as established by employing the modified single loop calculation of Li and Liu [3], had been predicted by Armstrong and Smith [40]. Hall-Petch behavior, as measured by elastic strains, has been reported to extend down to $\ell \approx 3 \text{ nm}$ for nanotwinned gold nanowires of 12 and 20 nm diameter [41]. Strength and strain rate sensitivity measurements have been reported for an axially-aligned, penta-twinned, structure in silver nanowires of 5 to 30 nm diameter [42]. Other related copper bicrystal micropillar experiments had been reported in which an axial coherent twin boundary was produced by a focused ion beam processing method and compressed in a nanoindentation test system to reveal, with reference to H-P model interpretation, the action of slip system transfer across the boundary [43]. Comparable nano-scale experiments and analyses have been reported as well for other micropillar materials, including "smaller is stronger" results for submicron aluminum specimens exhibiting an instability that was suppressed by the introduction of grain boundaries and secondary precipitate particles leading to flow stress levels exceeding 1.0 GPa [44].

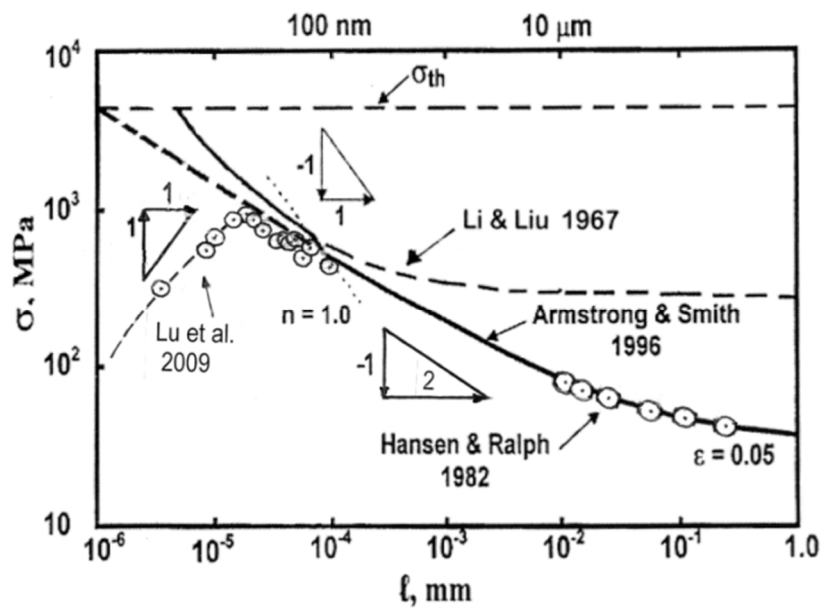


Figure 3. The flow stress dependence on grain size and nano-twin spacing for copper materials also relating to the transition from an $(1/\ell)^{1/2}$ to a $(1/\ell)$ dependence at ~ 100 nm and then to grain size weakening behavior at ~ 20 nm.

3.2. Nanograin Size Weakening

In Figure 3, grain size weakening is shown to occur for the nanotwinned copper material at $\ell \leq \sim 20$ nm [33]. The observation is attributed to deformation occurring principally in the grain boundary region, for example, by grain boundary sliding [45]. A general type of constitutive equation, that was originally developed to include measurements made on grain boundary weakening behavior observed in high temperature creep-type experiments, has been expressed for the observation in terms of strain rate dependence, $(d\varepsilon/dt)$ as

$$(d\varepsilon/dt) = (AD_L Gb/k_B T)(b/\ell)^p (\sigma/G)^q \quad (5)$$

In Equation (5), D_L is an appropriate boundary diffusion coefficient, k_B is Boltzmann's constant, T is temperature, and A and exponents, p and q , are experimental constants, in the latter case, taking on values of 1.0 or 2.0. In Figure 3, for example, $p/q = 1.0$. More recently, the equation has been applied to a range of nano-scale measurements made on nano-grain nickel materials for which the strain rate dependence of the plastic flow stress has been monitored in terms of a dimensional "activation volume", $v^* = A^*b$, parameter for which A^* is the thermal activation area and b is in the plane of A^* as

$$v^* = A^*b = k_B T [\partial \{\ln(d\varepsilon/dt)\} / \partial \tau_{Th}]_T \quad (6)$$

In Equation (6), the change in stress, $\partial \tau_{Th}$, accompanying an imposed change in strain rate is taken to be a thermal component of stress. Furthermore, the value of τ_{Th} in the fcc k_ε is thermally-activated and so depends on the strain rate in the same manner as applies for the value of $\sigma_{0\varepsilon}$. On such basis, an apparent H-P type dependence for the reciprocal value of v^* is obtained from both Equation (2) H-P $\sigma_{0\varepsilon}$ and k_ε terms as

$$(1/v^*) = (1/v^*)_0 + (k_\varepsilon/2m_T \tau_{C\varepsilon} v_C^*) \ell^{-1/2} \quad (7)$$

Figure 4 shows a compilation of $(1/v^*)$ measurements for conventional and nano-scale nickel materials [46–49]. The measurements follow an H-P type dependence because of the constant value of $\tau_{C\varepsilon} v_C^*$, at least at small strains [50]. Additional grain size weakening measurements have been added to the figure. Whereas, the $(1/v^*)$ values are shown to increase by an order of magnitude

between conventional and nano-scale grain sizes, there is an additional order-of-magnitude increase to atomic-scale dimensions for the grain size weakening behavior that itself is strain rate dependent, as demonstrated in Figure 4 for connection of the lower ($1/v^*$) value for the 40 nm grain size material tested at $(d\varepsilon/dt) = 1.04 \text{ s}^{-1}$ as compared with the higher value at a creep-connected strain rate 10^{-5} times slower [49]. Calculated values of v^* from Equation (6) showed an agreement with the additional increase in order of magnitude measurements [50]. These higher nano-scale dimensions seem reasonable with respect to individual atomic displacements being associated with grain boundary shearing deformations.

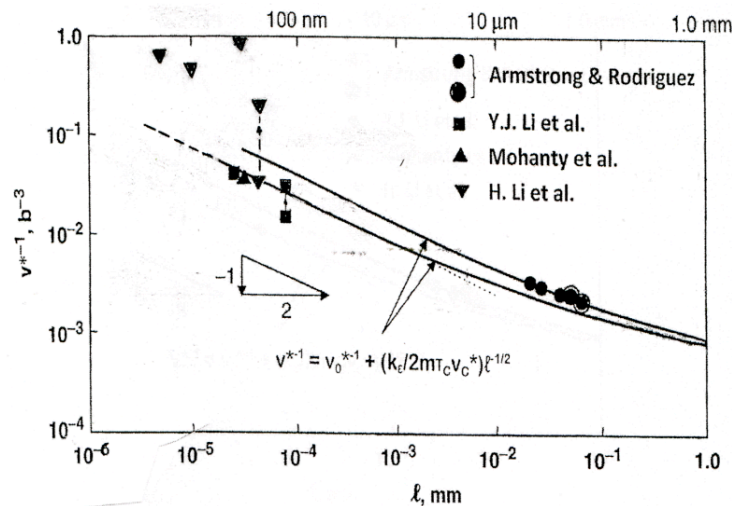


Figure 4. An H-P dependence for $(1/v^*)$ measurements made on nickel materials including nano-scale grain size strengthening and weakening measurements; the upper curve is at 77 K and lower one, 300 K.

4. Discussion

Of course, there are other important materials to consider beyond bcc iron and steel and the fcc aluminum, copper, and nickel materials, for which most crystal size dependent strength measurements and analyses have been made. A H-P dependence and the corresponding crystal size effect are known to be important for hcp metals because of the restricted number of slip or deformation twinning systems that are available to effect the accommodation and transmission of plastic flow at the crystal boundaries [9]. As an example, Kumar, Beyerlein, and Tomé have reported on grain size constraints against twin expansion for hcp materials, such as magnesium, whose H-P dependence has been investigated in detail relative to variously processing developed crystal orientation-dependent textures [51]. Even for nano-crystal fcc metals, Yuan, Beyerlein, and Zhou have presented reasonably quantitative evidence of concern for a crystallographic texture influence on $\sigma_{0\varepsilon}$ and k_e [52].

Much research has been done on α -titanium materials. Discrimination between the strengthening aspects of low-angle grain boundaries, whose misorientation, $\Delta\theta$, is accounted for in terms of the dislocation content, and in terms of accompanying high-angle grain boundaries, which are accounted for in terms of combined dislocations and coincident site lattice (CSL) matching, has been described for H-P results obtained by SPD processing of pure titanium [53]. X-ray Laue micro-diffraction and high angular resolution, electron back-scatter, diffraction measurements have been made on titanium to reveal locally the mis-orientations of adjacent grains, across which the forward stress concentrations of unrelaxed dislocation pile-ups could be correlated with the EFN model analysis [54,55]. Bond and Zikry have described a framework for dislocation pile-ups at grain boundaries spanning CSL and random structures [56].

Other materials are of interest as well. For example, a recent report has described observation of an exceptional grain boundary strengthening for nanocrystalline oxide materials [57]. The strength properties of other unidirectionally-solidified superalloy eutectic systems [19] and more complex eutectoid [58] and micro-laminated superalloy [59] material strength properties have been shown to follow a H-P dependence. Such strengthening in the Co crystal-matrix-constrained, composite WC-Co, cemented carbide system is well-known and was most recently illustrated by the application of nanoindentation hardness measurements [60].

Other material properties than strength are also affected by the same crystal size dependencies that have been described in the present case. An increase in mechanical toughness has been attributed to nano-scale silicon crystal thin films, nanospheres, and nanopillar type materials [61] mentioned at the beginning of the current report [2,4]. Valiev et al. [22–24] have described a full range of strength and related material properties that are improved at nano-scale dimensions. A sample report on the importance of taking material size into account in micro-scale deformation and fabrication processing of metal components is given in [62].

5. Summary

Comparative strength levels have been presented and assessed for nano-scale test measurements made on individual nanoparticles and nanopolycrystalline materials. An inverse crystal size dependence applies for individual, defect-free, particles, and is attributed to resisted dislocation nucleation at the particle surfaces, with or without the influence of an oxide layer. A H-P type reciprocal square root of grain size dependence, that applies quite generally at conventional and micro-scale polycrystal grain sizes, is shown on the basis of a supporting dislocation pile-up description to transition to a reciprocal size dependence in the nano-scale regime. Otherwise, current references are provided for wide employment of the pile-up model. An analogous Hall-Petch dependence for the reciprocal thermal “activation volume”, $(1/v^*)$, parameter, which exhibits a same order-of-magnitude increase in value over conventional-to-micro-scale grain sizes, is shown to increase by a further order of magnitude in the tens of nm grain size weakening regime, depending on the applied strain rate. Thus, v^* presents itself as a sensitive marker for monitoring the strengthening or weakening of nanopolycrystals.

Conflicts of Interest: The authors declare no conflict of interest.

Abbreviations

The following abbreviations are used in this manuscript:

H-P	Hall-Petch
EFN	Eshelby, Frank and Nabarro
ECAP	Equal channel angular pressing
SPD	Severe plastic deformation
CSL	Coincident site lattice

References

1. Han, W.Z.; Huang, L.; Ogata, S.; Kimizuka, H.; Yang, Z.C.; Weinberger, C.; Li, Q.J.; Liu, B.Y.; Zhang, X.X.; Li, J.; et al. From “Smaller is Stronger” to “Size-Independent Strength Plateau”: Towards Measuring the Ideal Strength of Iron. *Adv. Mater.* **2015**, *27*, 3385–3390. [[CrossRef](#)] [[PubMed](#)]
2. Nowak, J.D.; Beaver, A.R.; Ugurlu, O.; Girshick, S.L.; Gerberich, W.W. Small size strength dependence on dislocation nucleation. *Scr. Mater.* **2010**, *62*, 819–822. [[CrossRef](#)]
3. Li, J.C.M.; Liu, G.C.T. Circular dislocation pile-ups: I. Strength of ultrafine polycrystalline aggregates. *Philos. Mag.* **1967**, *15*, 1059–1063. [[CrossRef](#)]
4. Hintsala, E.D.; Wagner, A.J.; Gerberich, W.W.; Mkhoyan, K.A. The role of back stress in sub-50 nm Si nanocubes. *Scr. Mater.* **2016**, *114*, 51–55. [[CrossRef](#)]

5. Eshelby, J.D.; Frank, F.C.; Nabarro, F.R.N. The equilibrium of linear arrays of dislocations. *Philos. Mag.* **1951**, *42*, 351–364. [[CrossRef](#)]
6. Hall, E.O. The deformation and ageing of mild steel: III. Discussion of results. *Proc. Phys. Soc. Sect. B* **1951**, *64*, 747–753. [[CrossRef](#)]
7. Petch, N.J. The cleavage strength of polycrystals. *J. Iron Steel Inst.* **1953**, *174*, 25–28.
8. Smith, T.R.; Armstrong, R.W.; Hazzledine, P.M.; Masamura, R.A.; Pande, C.S. Pile-Up Based Hall-Petch Consideration at Ultra-Fine Grain Sizes. In *Grain Size and Mechanical Properties—Fundamentals and Applications*; Otonari, M.A., Armstrong, R.W., Grant, N.J., Ishizaki, K., Eds.; Materials Research Society: Pittsburgh, PA, USA, 1995; Volume 362, pp. 31–37.
9. Armstrong, R.W.; Codd, I.; Douthwaite, R.M.; Petch, N.J. The plastic deformation of polycrystalline aggregates. *Philos. Mag.* **1962**, *7*, 45–58. [[CrossRef](#)]
10. Purcek, G.; Saray, O.; Karaman, I.; Maier, H.J. High strength and high ductility in ultrafine-grained interstitial-free steel produced by ECAE and annealing. *Metall. Mater. Trans. A* **2012**, *43*, 1884–1894. [[CrossRef](#)]
11. Jang, J.C.S.; Koch, C.C. The Hall-Petch relationship in nanocrystalline iron produced by ball milling. *Scr. Metall.* **1990**, *24*, 1599–1604. [[CrossRef](#)]
12. Embury, J.D.; Fisher, R.M. The structure and properties of drawn pearlite. *Acta Metall.* **1966**, *14*, 147–152. [[CrossRef](#)]
13. Zhang, X.D.; Godfrey, A.; Huang, X.; Hansen, N.; Liu, Q. Microstructure and strengthening mechanisms in cold-drawn pearlitic steel wire. *Acta Mater.* **2011**, *59*, 3422–3430. [[CrossRef](#)]
14. Li, Y.; Raabe, D.; Herbig, M.; Choi, P.P.; Goto, S.; Kostka, A.; Yarita, H.; Borchers, C.; Kirchheim, R. Segregation stabilizes nanocrystalline bulk steel with near theoretical strength. *Phys. Rev. Lett.* **2014**, *113*, 106104. [[CrossRef](#)] [[PubMed](#)]
15. Armstrong, R.W. Hall-Petch k dependencies in nanopolycrystals. *Emerg. Mater. Res.* **2014**, *3*, 246–251. [[CrossRef](#)]
16. Svoboda, J.; Zickler, G.A.; Kozeschnik, E.; Fischer, F.D. Kinetics of interstitial segregation in Cottrell atmospheres and grain boundaries. *Philos. Mag. Lett.* **2015**, *95*, 458–465. [[CrossRef](#)]
17. Kang, J.H.; Duan, S.; Kim, S.J.; Bleck, W. Grain boundary strengthening in high Mn austenitic steels. *Metall. Mater. Trans. A* **2016**, *47A*, 1918–1921. [[CrossRef](#)]
18. Fitzgerald, S.P.; Dudarev, S.L. Dislocation pile-ups in Fe at high temperatures. *Proc. R. Soc. A* **2008**, *464*, 2549–2559. [[CrossRef](#)]
19. Armstrong, R.W. The yield and flow stress dependence on polycrystal grain size. In *Yield, Flow and Fracture of Polycrystals*; Baker, T.N., Ed.; Applied Science Publisher: London, UK, 1983; pp. 1–31.
20. Langford, G. Deformation of pearlite. *Metall. Trans. A* **1977**, *8A*, 861–875. [[CrossRef](#)]
21. Muñoz, J.A.; Higuera, O.F.; Cabrera, J.M. Microstructural and mechanical study in the plastic zone of ARMCO iron processed by ECAP. *Mater. Sci. Eng. A* **2017**, *697*, 24–36. [[CrossRef](#)]
22. Valiev, R.Z.; Estrin, Y.; Horita, Z.; Langdon, T.G.; Zehetbauer, M.J.; Zhu, Y. Producing bulk ultrafine—Grained materials by severe plastic deformation: Ten years later. *JOM* **2016**, *68*, 1216–1226. [[CrossRef](#)]
23. Valiev, R.Z.; Estrin, Y.; Horita, Z.; Langdon, T.G.; Zehetbauer, M.J.; Zhu, Y.T. Fundamentals of superior properties in bulk nano SPD materials. *Mater. Res. Lett.* **2016**, *4*, 1–21. [[CrossRef](#)]
24. Karavaeva, M.V.; Kiseleva, S.K.; Ganeev, A.V.; Protasova, E.O.; Ganiev, M.M.; Simonova, L.A.; Valiev, R.Z. Superior strength of carbon steel with an ultrafine-grained microstructure and its enhanced thermal stability. *J. Mater. Sci.* **2015**, *50*, 6730–6738. [[CrossRef](#)]
25. Field, D.M.; Van Aken, D.C. Nanocrystalline advanced high strength steel produced by cold rolling and annealing. *Metall. Mater. Trans. A* **2016**, *47A*, 1912–1917. [[CrossRef](#)]
26. He, B.B.; Hu, B.; Yen, H.W.; Cheng, G.J.; Wang, Z.K.; Luo, H.W.; Huang, M.X. High dislocation density-induced large ductility in deformed and partitioned steels. *Science* **2017**, *357*, 1029–1032. [[CrossRef](#)] [[PubMed](#)]
27. Feruz, Y.; Mordehai, D. Towards a universal size-dependent strength of face-centered cubic nanoparticles. *Acta Mater.* **2016**, *103*, 433–441. [[CrossRef](#)]
28. Carreker, R.P., Jr.; Hibbard, W.R., Jr. Tensile deformation of aluminum as a function of temperature, strain rate and grain size. *Trans. TMS-AIME* **1957**, *209*, 1157–1163.

29. Tsuji, N.; Ito, Y.; Saito, Y.; Minamino, Y. Strength and ductility of ultrafine grained aluminum and iron produced by ARB and annealing. *Scr. Mater.* **2002**, *47*, 893–899. [[CrossRef](#)]
30. Keller, C.; Hug, E. Hall-Petch behavior of Ni polycrystals with a few grains per thickness. *Mater. Lett.* **2008**, *62*, 1718–1720. [[CrossRef](#)]
31. Torrents, A.; Yang, H.; Mohamed, F. Effect of annealing on hardness and the modulus of elasticity in bulk nanocrystalline nickel. *Metall. Mater. Trans. A* **2010**, *41A*, 621–630. [[CrossRef](#)]
32. Hansen, N.; Ralph, B. The strain and grain size dependence of the flow stress of copper. *Acta Metall.* **1982**, *30*, 411–417. [[CrossRef](#)]
33. Lu, L.; Chen, X.; Huang, X.; Lu, K. Revealing the maximum strength in nanotwinned copper. *Science* **2009**, *323*, 607–610. [[CrossRef](#)] [[PubMed](#)]
34. Armstrong, R.W. Hall-Petch description of nanopolycrystalline Cu, Ni and Al strength levels and strain rate sensitivities. *Philos. Mag.* **2016**, *96*, 3097–3108. [[CrossRef](#)]
35. Kapp, M.W.; Kirchlechner, C.; Pippan, R.; Dehm, G. Importance of dislocation pile-ups on the mechanical properties and the Bauschinger effect in microcantilevers. *J. Mater. Res.* **2015**, *30*, 791–797. [[CrossRef](#)]
36. Aifantis, K.E.; Soer, W.A.; De Hosson, J.T.M.; Willis, J.R. Interfaces within strain gradient plasticity: Theory and experiments. *Acta Mater.* **2006**, *54*, 5077–5085. [[CrossRef](#)]
37. Xiao, X.; Terentyev, D.; Chen, Q.; Yu, L.; Chen, L.; Bakaev, A.; Duan, H. The depth dependent hardness of bicrystals with dislocation transmission through grain boundaries: A theoretical model. *Int. J. Plast.* **2017**, *90*, 212–230. [[CrossRef](#)]
38. Zhang, C.; Voyiadjis, G.Z. Rate-dependent size effects and material length scales in nanoindentation near the grain boundary for a bicrystal FCC metal. *Mater. Sci. Eng. A* **2016**, *659*, 55–62. [[CrossRef](#)]
39. Li, Z.; Hou, C.; Huang, M.; Ouyang, C. Strengthening mechanisms in micro-polycrystals with penetrable grain boundaries by discrete dislocation dynamics simulation and Hall-Petch effect. *Comput. Mater. Sci.* **2009**, *46*, 1124–1134. [[CrossRef](#)]
40. Armstrong, R.W.; Smith, T.R. Dislocation pile-up predictions for the strength properties of ultrafine grain size fcc metals. In *Processing and Properties of Nanocrystalline Materials*; Suryanarayana, C., Singh, J., Froes, F.H., Eds.; TMS-AIME: Warrendale, PA, USA, 1996; pp. 345–354.
41. Wang, J.; Sansoz, F.; Deng, C.; Xu, G.; Han, G.; Mao, S.X. Strong Hall-Petch type behavior in the elastic strain limit of nanotwinned gold nanowires. *Nano Lett.* **2015**, *15*, 3865–3870. [[CrossRef](#)] [[PubMed](#)]
42. Zhang, X.; Li, X.; Gao, H. Size and strain rate effects in tensile strength of penta-twinned Ag nanowires. *Acta Mech. Sin.* **2017**, *33*, 792–800. [[CrossRef](#)]
43. Hirouchi, T.; Shibutani, Y. Mechanical responses of copper bicrystalline micro pillars with $\Sigma 3$ coherent twin boundaries by uniaxial compression test. *Mater. Trans.* **2014**, *55*, 52–57. [[CrossRef](#)]
44. Hu, T.; Jiang, L.; Yang, H.; Ma, K.; Topping, T.D.; Yee, J.; Li, M.; Mukherjee, A.K.; Schoenung, J.M.; Lavernia, E.J. Stabilized plasticity in ultrahigh strength, submicron Al crystals. *Acta Mater.* **2015**, *94*, 46–58. [[CrossRef](#)]
45. Langdon, T.G. Grain boundary sliding revisited: Developments in sliding over four decades. *J. Mater. Sci.* **2006**, *41*, 597–609. [[CrossRef](#)]
46. Armstrong, R.W.; Rodriguez, P. Flow stress/grain size/strain rate coupling for fcc nanopolycrystals. *Philos. Mag.* **2006**, *86*, 5787–5796. [[CrossRef](#)]
47. Li, Y.J.; Mueller, H.W.; Höppel, M.; Göken, M.; Blum, W. Deformation kinetics of nanocrystalline nickel. *Acta Mater.* **2007**, *55*, 5708–5717. [[CrossRef](#)]
48. Mohanty, G.; Wheeler, J.M.; Raghavan, R.; Wehrs, J.; Hasgawa, M.; Mischler, S.; Phillippe, L.; Michler, J. Elevated temperature, strain rate jump microcompression of nanocrystalline nickel. *Philos. Mag.* **2015**, *95*, 1878–1895. [[CrossRef](#)]
49. Li, H.; Liang, Y.; Zhao, L.; Hu, J.; Han, S.; Lian, J. Mapping the strain rate and grain size dependence of deformation behaviors in nanocrystalline face-centered-cubic Ni and Ni-based alloys. *J. Alloy. Compd.* **2017**, *709*, 566–574. [[CrossRef](#)]
50. Armstrong, R.W.; Balasubramanian, N. Unified Hall-Petch description of nano-grain nickel hardness, flow stress and strain rate sensitivity measurements. *AIP Adv.* **2017**, *7*, 85010. [[CrossRef](#)]
51. Kumar, M.A.; Beyerlein, I.J.; Tomé, C.N. Grain size constraints on twin expansion in hexagonal close packed crystals. *J. Appl. Phys.* **2016**, *120*, 155105. [[CrossRef](#)]

52. Yuan, R.; Beyerlein, I.J.; Zhou, C. Coupled crystal orientation-size effects on the strength of nano crystals. *Nat. Sci. Rep.* **2016**, *6*, 26254. [[CrossRef](#)] [[PubMed](#)]
53. Luo, P.; Hu, Q.; Wu, X. Quantitatively analyzing strength contribution vs grain boundary scale relation in pure titanium subjected to severe plastic deformation. *Metal. Mater. Trans. A.* **2016**, *47A*, 1922–1927. [[CrossRef](#)]
54. Britton, T.B.; Wilkinson, A.J. Stress fields and geometrically necessary dislocation density distributions near the head of a blocked slip band. *Acta Mater.* **2012**, *60*, 5773–5782. [[CrossRef](#)]
55. Guo, Y.; Collins, D.M.; Tarleton, E.; Hofmann, F.; Tischler, J.; Liu, W.; Xu, R.; Wilkinson, A.J.; Britton, T.B. Measurements of stress fields near a grain boundary: Exploring blocked arrays of dislocations in 3D. *Acta Mater.* **2015**, *96*, 229–236. [[CrossRef](#)]
56. Bond, D.M.; Zikry, M.A. A predictive framework for dislocation-density pile-ups in crystalline systems with coincident site lattice and random grain boundaries. *J. Eng. Mater. Technol.* **2017**, *139*, 021023. [[CrossRef](#)]
57. Muche, D.N.F.; Drazin, J.W.; Mardinly, J.; Dey, S.; Castro, R.H.R. Colossal grain boundary strengthening in ultrafine nanocrystalline oxides. *Mater. Lett.* **2017**, *186*, 298–300. [[CrossRef](#)]
58. Baker, I.; Meng, F. Lamellar coarsening in $\text{Fe}_{28}\text{Ni}_{18}\text{Mn}_{33}\text{Al}_{21}$ and its influence on room temperature tensile behavior. *Acta Mater.* **2015**, *95*, 124–131. [[CrossRef](#)]
59. Fan, G.; Wang, Q.; Geng, L.; Zhang, J.; Hu, W.; Du, Y. Fabrication, microstructure, and mechanical property of NiAl-based composite with microlaminated architecture by roll bonding and annealing treatment. *Metall. Mater. Trans. A* **2016**, *47A*, 1280–1291. [[CrossRef](#)]
60. Roa, J.J.; Jiménez-Piqué, E.; Tarragó, J.M.; Sandoval, D.A.; Mateo, A.; Fair, J.; Llanes, L. Hall-Petch strengthening of the constrained metallic binder in WC-Co cemented carbides: Experimental assessment by means of massive nanoindentation and statistical analysis. *Mater. Sci. Eng. A* **2016**, *676*, 487–491. [[CrossRef](#)]
61. Beaber, A.R.; Nowak, J.D.; Ugurlu, O.; Mook, W.M.; Girschick, S.L.; Ballarina, R.; Gerberich, W.W. Smaller is tougher. *Philos. Mag.* **2011**, *91*, 1179–1189. [[CrossRef](#)]
62. Fu, M.W.; Wang, J.L.; Korsunsky, A.M. A review of geometrical and microstructural size effects in micro-scale deformation processing of metallic alloy components. *Int. J. Mach. Tools Manuf.* **2016**, *109*, 94–125. [[CrossRef](#)]



© 2017 by the author. Licensee MDPI, Basel, Switzerland. This article is an open access article distributed under the terms and conditions of the Creative Commons Attribution (CC BY) license (<http://creativecommons.org/licenses/by/4.0/>).